J|A|C|S ARTICLES

Published on Web 02/16/2010

Multiple Bistability and Tristability with Dual Spin-State Conversions in $[Fe(dpp)_2][Ni(mnt)_2]_2 \cdot MeNO_2$

Masayuki Nihei, Hirotaka Tahira, Nobukazu Takahashi, Yusuke Otake, Yasuhisa Yamamura, Kazuya Saito, and Hiroki Oshio*

Graduate School of Pure and Applied Sciences, University of Tsukuba, Tennodai 1-1-1, Tsukuba, Ibaraki 305-8571, Japan

Received November 30, 2009; E-mail: oshio@chem.tsukuba.ac.jp

Abstract: The multicomponent system of $[Fe(dpp)_2][Ni(mnt)_2]_2 \cdot MeNO_2$ (**1**; dpp = 2,6-bis(pyrazol-1-yl)pyridine and mnt = maleonitriledithiolate) was prepared by the reaction of $[Fe(dpp)_2](BF_4)_2$ with $(Bu_4N)[Ni(mnt)_2]$ in $MeNO_2$. Variable-temperature X-ray structural analyses, magnetic susceptibility, and heat capacity measurements confirmed that **1** undergoes multiple spin-state conversions in both the cationic and anionic components. The asymmetric unit in the crystal contains one $[Fe(dpp)_2]^{2+}$ cation, two $[Ni(mnt)_2]^-$ anions ($[Ni1]^-$ and $[Ni2]^-$), and one solvent molecule. Magnetic susceptibility measurements revealed that a paramagnetic state in the high-temperature region (HT phase) was abruptly converted to a diamagnetic low-temperature (LT) phase below 180 K as the temperature was lowered from 270 K. As the temperature was raised from 125 to 270 K, successive phase transitions occurred to the HT phase via intermediate phases (IM1, IM2, and IM3) at 175.5, 186.5, 194.0, and 244.0 K, respectively. In the HT phase $[Fe(dpp)_2]^{2+}$ is in the high-spin state, and each $[Ni1]^-$ and $[Ni2]^-$ moiety is arranged in monomeric form with an $S = {}^1/_2$ spin ground state. In the LT phase $[Fe(dpp)_2]^{2+}$ is in the low-spin state and the nickel moieties are dimerized and diamagnetic. In the IM1 and IM2 phases the iron(II) sites are partially in the HS state and both $[Ni]^-$ moieties are dimeric, as suggested by ^{57}Fe Mössbauer measurements. In the IM3 phase, $[Fe(dpp)_2]^{2+}$ is in the HS state and the anions exist in both their monomeric ($[Ni1]^-$) and dimeric ($[Ni2]^-$) forms. Rapid thermal quenching from 300 to 5 K yielded a metastable HS phase, which relaxed to the LT phase via the IM1 phase as the temperature was raised to 150 K. A partial light induced spin transition on the iron site was observed at 5 K.

Introduction

A bistable system can exist in two phases at a given temperature, both of which have minimum free energy, and two phases can be switched by applying external stimuli.[1] Iron(II) complexes can exhibit high-spin (HS, $S = 2$) and low-spin (LS, $S = 0$) states depending on ligand field strength. In complexes of appropriate ligand field strength, iron(II) centers can undergo a thermally induced spin transition between HS and LS states at a certain temperature, acting as spin-crossover (SCO) materials. Some SCO complexes, exhibiting an abrupt phase transition with thermal hysteresis, have two stable spin states at the same temperature, and the two states can be switched by external stimuli.[2] $[Fe^{II}(dpp)_2]X_2$ (dpp = 2,6-bis(pyrazol-1-yl)pyridine) is one of the most studied SCO complexes (Scheme 1). The SCO behavior of $[Fe^{II}(dpp)_2]X_2$ is associated with relatively large structural changes, and the temperature profiles of the spin-state conversions depend on the counteranions.[3]

Scheme 1. Structures of $[Fe(dpp)_2]^{2+}$ and $[Ni(mnt)_2]^-$

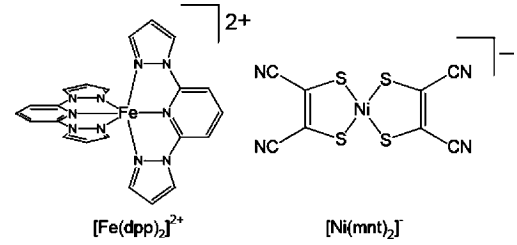

Some organic and organometallic radicals are, on the other hand, good candidates for magnetically bistable systems.[4] An

(1) (a) Irie, M. *Chem. Rev.* **2000**, *40*, 1685. (b) Pease, A. R.; Jeppesen, J. O.; Stoddart, J. F.; Juo, Y.; Collier, C. P.; Heath, J. R. *Acc. Chem. Res.* **2001**, *34*, 433. (c) Niel, V.; Thompson, A. L.; Muñoz, M. C.; Galet, A.; Goeta, A. E.; Real, J. A. *Angew. Chem., Int. Ed.* **2003**, *42*, 3760. (d) Dei, A.; Gatteschi, D.; Sangregorio, C.; Sorace, L. *Acc. Chem. Res.* **2004**, *37*, 827. (e) Migliori, J. M.; Reiff, W. M.; Arif, A. M.; Miller, J. S. *Inorg. Chem.* **2004**, *43*, 6875. (f) Sato, O.; Iyoda, T.; Fujishima, A.; Hahimoto, K. *Science* **1996**, *271*, 49. (g) Feringa, B. L. *Acc. Chem. Res.*; **2001**, *34*, 504. (h) Sato, O. *Acc. Chem. Res.* **2003**, *36*, 692. (i) Kosaka, W.; Nomura, K.; Hashimoto, K.; Ohkoshi, S. *J. Am. Chem. Soc.* **2005**, *127*, 8590.

(2) (a) Gütlich, P.; Hauser, A.; Spiering, H. *Angew. Chem., Int. Ed.* **1994**, *33*, 2024. (b) Kahn, O.; Martinez, C. J. *Science* **1998**, *279*, 44. (c) Gütlich, P., Goodwin, H. A., Eds. *Spin Crossover in Transition Metal Compounds I-III*; Springer: New York, 2004; Topics in Current Chemistry, pp 233−235. (d) Real, J. A.; Gaspar, A. B.; Muñoz, M. C. *Dalton Trans.* **2005**, 2062. (e) Gütlich, P.; Garcia, Y.; Woike, T. *Coord. Chem. Rev.* **2001**, *219*−*221*, 839. (f) Real, J. A.; Gaspar, A. B.; Niel, V.; Muñoz, M. C. *Coord. Chem. Rev.* **2003**, *236*, 121. (g) Neville, S. M.; Halder, G. J.; Chapman, K. W.; Duriska, M. B.; Moubaraki, B.; Murray, K. S.; Kepert, C. J. *J. Am. Chem. Soc.* **2008**, *131*, 12106. (h) Southon, P. D.; Liu, L.; Fellows, E. A.; Price, D. J.; Halder, G. J.; Chapman, K. W.; Moubaraki, B.; Murray, K. S.; Létard, J. F.; Kepert, C. J. *J. Am. Chem. Soc.* **2009**, *131*, 10998.

organic radical of 1,3,5-trithia-2,4,6-triazapentalenyl showed a transition between paramagnetic monomer and diamagnetic dimer phases associated with large thermal hysteresis.[5] Square-planar metal complexes with dithiolenes tend to form 1D to 3D structures, and some molecular crystals have been reported to exhibit high electric conductivity and ferromagnetism.[6] Recently, magnetic bistability with distinct paramagnetic and diamagnetic phases has been observed in (RbzPy)[Ni(mnt)$_2$] (RbzPy = 4-R-benzylpyridinium and mnt = maleonitriledithiolate), where almost uniform chain structures composed of π-stacked paramagnetic radical anions undergo dimerization by the Spin-Pierls-like distortion, leading to singlet states.[7]

Bistable materials are considered to be good candidates for molecular devices, such as sensors, switches, and memories.[8] A *multiply bistable* system is defined as ones with bistability at some temperatures, and a *tristable* system has three stable phases at a given temperature. Such systems can be used as new molecular devices such as multiswitch and ternary memory. Multistepped spin-state conversions have been observed in monomeric and multidimensional polymeric SCO complexes.[9] [Fe(pic)$_3$]Cl$_2$(solvent) is one of the most studied two-step SCO systems, and X-ray diffraction and heat capacity measurements revealed that iron(II) SCO sites formed a long-range periodic structure with an HS:LS ratio of 1:1.[10] Polynuclear SCO complexes, which have two or more SCO chromophores in a molecule, are promising candidates for a system exhibiting multistepped spin transitions, and some dinuclear and tetranuclear SCO complexes have been reported to show two-stepped SCO behavior.[11] However, the number of multiply bistable molecules, exhibiting multistepped spin transitions with thermal hysteresis, is still limited.[12] Multicomponent materials in which each component has a different magnetic bistability are also expected to be multiply bistable compounds with multistepped phase transitions. Multistepped giant hysteresis was confirmed in [Cp$_2$M][Ni(L)$_2$] (M = Fe, Co; L = asymmetric dithiolate ligand; Cp = cyclopentadiene),[13] in which structural phase transitions of complex anions were associated with the rotational disorder of the cyclopentadienyl rings.[14] We report here unprecedented dual spin-state conversions in [Fe(dpp)$_2$]-[Ni(mnt)$_2$]$_2$·MeNO$_2$ (**1**), composed of a SCO cation and anion radicals, in which SCO at iron(II) sites is strongly coupled with monomer−dimer structural phase transitions in the Ni complex anions. Heat- and light-induced phase transitions are discussed in detail.

Experimental Section

Synthesis. All reagents were obtained from commercial suppliers and were used without further purification. [Fe(dpp)$_2$](BF$_4$)$_2$ and (Bu$_4$N)[Ni(mnt)$_2$] were synthesized according to literature methods.[15,16]

(3) (a) Carbonera, C.; Costa, J. S.; Money, V. A.; Elhaïk, J.; Howard, J. A. K.; Halcrow, M. A.; Létard, J.-F. *Dalton Trans.* **2006**, 3058. (b) Money, V. A.; Elhaïk, J.; Halcrow, M. A.; Howard, J. A. K. *Dalton Trans.* **2004**, 1516. (c) Halcrow, M. A. *Coord. Chem. Rev.* **2005**, *249*, 2880. (d) Money, V. A.; Carbonera, C.; Elhaïk, J.; Halcrow, M. H.; Howard, J. A. K.; Létard, J.-F. *Chem. Eur. J.* **2007**, *13*, 5503. (e) Nihei, M.; Han, L.; Oshio, H. *J. Am. Chem. Soc.* **2007**, *129*, 5312. (f) Rajadurai, C.; Schramm, F.; Fuhr, O.; Ruben, M. *Eur. J. Inorg. Chem.* **2008**, 2649.

(4) (a) Itkis, M. E.; Chi, X.; Cordes, A. W.; Haddon, R. C. *Science* **2002**, *296*, 1443. (b) Brusso, J. L.; Clements, O. P.; Haddon, R. C.; Itkis, M. E.; Leitch, A. A.; Oakley, R. T.; Reed, R. W.; Richardson, J. F. *J. Am. Chem. Soc.* **2004**, *126*, 8256. (c) Sorai, M.; Nakano, M.; Miyazaki, Y. *Chem. Rev.* **2006**, *106*, 976.

(5) Fujita, W.; Awaga, K. *Science* **1999**, *286*, 261.

(6) (a) Robertson, N.; Cronin, L. *Coord. Chem. Rev.* **2002**, *227*, 93. (b) Cassoux, P.; Valade, L.; Kobayashi, H.; Kobayashi, A.; Clark, R. A.; Underhill, A. E. *Coord. Chem. Rev.* **1991**, *110*, 115. (c) Cassoux, P. *Coord. Chem. Rev.* **1999**, *185*, 213. (d) Tanaka, H.; Okano, Y.; Kobayashi, H.; Suzuki, W.; Kobayashi, A. *Science* **2001**, *291*, 285. (e) Coronado, E.; Galán-Mascarós, J. R.; Gómez-García, C. J.; Laukhin, V. *Nature* **2000**, *408*, 447.

(7) (a) Xie, J.; Ren, X.; Song, Y.; Zhang, W.; Liu, W.; He, C.; Meng, Q. *Chem. Commun.* **2002**, 2346. (b) Willet, R. D.; Gómez-García, C. J.; Ramakrishna, B. L.; Twamley, B. *Polyhedron* **2005**, *24*, 2232. (c) Ren, X. M.; Nishihara, S.; Akutagawa, T.; Noro, S.; Nakamura, T. *Inorg. Chem.* **2006**, *45*, 2229. (d) Ni, Z.; Ren, X.; Ma, J.; Xie, J.; Ni, C.; Chen, Z.; Meng, Q. *J. Am. Chem. Soc.* **2005**, *127*, 14330. (e) Ren, X. M.; Akutagawa, T.; Noro, S.; Nishihara, S.; Nakamura, T.; Yoshida, Y.; Inoue, K. *J. Phys. Chem. B* **2006**, *110*, 7671. (f) Ren, X.; Meng, Q.; Song, Y.; Lu, C.; Hu, C. *Inorg. Chem.* **2002**, *41*, 5686.

(8) (a) Balzani, V.; Françisco, A. C.; Raymo, M.; Sttodart, J. F. *Angew. Chem., Int. Ed.* **2000**, *39*, 3348. (b) Sato, O.; Tao, J.; Zhang, Y.-Z. *Angew. Chem., Int. Ed.* **2007**, *46*, 2152. (c) Bousseksou, A.; Molnár, G.; Matouzenko, G. *Eur. J. Inorg. Chem.* **2004**, *22*, 4353.

(9) (a) Neville, S. M.; Leita, B. A.; Halder, G. J.; Kepert, C. J.; Moubaraki, B.; Létard, J.-F.; Murray, K. S. *Chem. Eur. J.* **2008**, *14*, 10123. (b) Boinnard, D.; Bousseksou, A.; Dworkin, A.; Savariault, J.-M.; Varret, F.; Tuchagues, J.-P. *Inorg. Chem.* **1994**, *33*, 271. (c) Garcia, Y.; Kahn, O.; Rabardel, L.; Chansou, B.; Salmon, L.; Tuchagues, J. P. *Inorg. Chem.* **1999**, *38*, 4663. (d) Matouzenko, G. S.; Létard, J.-F.; Lecocq, S.; Bousseksou, A.; Capes, L.; Salmon, L.; Perrin, M.; Kahn, O.; Collet, A. *Eur. J. Inorg. Chem.* **2001**, 2935. (e) Rodriguez-Velamazán, J. A.; Castro, M.; Palacios, E.; Burriel, R.; Kitazawa, T.; Kawasaki, T. *J. Phys. Chem. B* **2007**, *111*, 1256. (f) Yamada, M.; Ooidemizu, M.; Ikuta, Y.; Osa, S.; Matumoto, N.; Iijima, S.; Kojima, M.; Dahan, F.; Tuchagues, J.-P. *Inorg. Chem.* **2003**, *42*, 8406. (g) Niel, V.; Muñoz, M. C.; Gaspar, A. B.; Galet, A.; Levchenko, G.; Real, J. A. *Chem. Eur. J.* **2002**, *8*, 2446. (h) Garcia, Y.; Kahn, O.; Rabardel, L.; Chansou, B.; Salmon, L.; Tuchagues, J. P. *Inorg. Chem.* **1999**, *38*, 4663. (i) Sato, T.; Nishi, K.; Iijima, S.; Kojima, M.; Matsumoto, N. *Inorg. Chem.* **2009**, *48*, 7211. (j) Halder, G. J.; Chapman, K. W.; Neville, S. M.; Moubaraki, B.; Murray, K. S.; Létard, J. F.; Kepert, C. J. *J. Am. Chem. Soc.* **2008**, *130*, 17552.

(10) (a) Chernshov, D.; Klinduhov, N.; Törnroos, K. W.; Hostettler, M.; Vangdal, B.; Bürgi, H.-B. *Phys. Rev. B* **2007**, *76*, 014406. (b) Hostettler, M.; Törnroos, K. W.; Chernyshov, D.; Vangdal, B.; Bürgi, H.-B. *Angew. Chem., Int. Ed.* **2004**, *43*, 4589. (c) Kaji, K.; Sorai, M. *Thermochim. Acta* **1985**, *88*, 185.

(11) (a) Bousseksou, A.; Molnár, G.; Real, J. A.; Tanaka, K. *Coord. Chem. Rev.* **2007**, *251*, 1822. (b) Gaspar, A. B.; Muñoz, M. C.; Real, J. A. *J. Mater. Chem.* **2006**, *16*, 2522. (c) Amoore, J. J. M.; Kepert, C. J.; Cahion, J. D.; Moubaraki, B.; Neville, S. M.; Murray, K. S. *Chem. Eur. J.* **2006**, *12*, 8220. (d) Nihei, M.; Ui, M.; Yokota, M.; Han, L.; Maeda, A.; Kishida, H.; Okamoto, H.; Oshio, H. *Angew. Chem., Int. Ed.* **2005**, *44*, 6484. (e) Nakano, K.; Kawata, S.; Yoneda, K.; Fuyuhiro, A.; Yagi, T.; Nasu, S.; Morimoto, S.; Kaizaki, S. *Chem. Commun.* **2004**, 2892. (f) Wu, D.-Y.; Sato, O.; Einaga, Y.; Duan, C.-Y. *Angew. Chem., Int. Ed.* **2009**, *48*, 1475.

(12) (a) Grunert, C. M.; Schweifer, J.; Weinberger, P.; Linert, W.; Mereiter, K.; Hilscher, G.; Muller, M.; Wiesinger, G.; van Koningsbruggen, P. J. *Inorg. Chem.* **2004**, *43*, 155. (b) Hayami, S.; Gu, Z.; Yoshiki, H.; Fujishima, A.; Sato, O. *J. Am. Chem. Soc.* **2001**, *123*, 11644. (c) Bonnet, S.; Molnár, G.; Costa, J. S.; Siegler, M. A.; Spek, A. L.; Bousseksou, A.; Fu, W.-T.; Gamez, P.; Reedijk, J. *Chem. Mater.* **2009**, *21*, 1123. (d) Bonnet, S.; Siegler, M. A.; Costa, J. S.; Molnár, G.; Bousseksou, A.; Spek, A. L.; Gamez, P.; Reedijk, J. *Chem. Commun.* **2008**, 5619.

(13) (a) Jeannin, O.; Clérac, R.; Fourmigué, M. *Chem. Mater.* **2007**, *19*, 5946. (b) Jeannin, O.; Clérac, R.; Fourmigué, M. *J. Am. Chem. Soc.* **2006**, *108*, 14649.

(14) (a) Dorbes, S.; Valade, L.; Real, J. A.; Faulmann, C. *Chem. Commun.* **2005**, 69. (b) Faulmann, C.; Dorbes, S.; Bonneval, B. G.; Molnár, G.; Bousseksou, A.; Gomez-Garcia, C. J.; Coronado, E.; Valade, L. *Eur. J. Inorg. Chem.* **2005**, 3261. (c) Takahashi, K.; Cui, H.-B.; Okano, Y.; Kobayashi, H.; Einaga, Y.; Sato, O. *Inorg. Chem.* **2006**, *45*, 5739. (d) Faulmann, C.; Jacob, K.; Dorbes, S.; Lampert, S.; Malfant, O.; Doublet, M.-L.; Valade, L.; Real, J. A. *Inorg. Chem.* **2007**, *46*, 8548. (e) Faulmann, C.; Dorbes, S.; Lampert, S.; Jacob, K.; Bonneval, B. G.; Molnár, G.; Bousseksou, A.; Real, J. A.; Valade, L. *Inorg. Chim. Acta* **2007**, *360*, 3870. (f) Takahashi, K.; Cui, H.-B.; Okano, Y.; Kobayashi, H.; Mori, H.; Tajima, H.; Einaga, Y.; Sato, O. *J. Am. Chem. Soc.* **2008**, *130*, 6688.

(15) Holland, J. M.; McAllister, J. A.; Kilner, C. A.; Thornton-Pett, M.; Bridgeman, A. J.; Halcrow, M. A. *Dalton Trans.* **2002**, 548.

(16) Davidson, D.; Holm, R. H. *Inorg. Synth.* **1967**, *10*, 8.

$[Fe(dpp)_2][Ni(mnt)_2]_2 \cdot MeNO_2$ (1). The reaction of $[Fe(dpp)_2](BF_4)_2$ (20 mg, 0.031 mmol) with $(Bu_4N)[Ni(mnt)_2]$ (46 mg, 0.078 mmol) in $MeNO_2$ (7 mL) gave a dark green solution. The resulting solution was allowed to stand at 5 °C to give black platelike crystals of **1** (23 mg, 0.019 mmol, yield of 61%). Anal. Calcd for $C_{39}H_{21}N_{19}FeNi_2O_2S_8$: C, 38.48; H, 1.74; N, 21.86. Found: C, 38.64; H, 1.75; N, 21.76.

Crystal Structure Analyses. A single crystal of **1** was mounted with epoxy resin on the tip on a glass fiber. Measurements were performed at 293, 200, and 140 K after cooling the crystal from 300 K (cooling mode) and at 180 and 205 K after heating from 140 K (heating mode). Crystallographic parameters are summarized in Table S1. Diffraction data were collected using a Bruker SMART APEX diffractometer equipped with a CCD type area detector. A full sphere of data was collected with graphite-monochromated Mo Kα radiation ($\lambda = 0.710\ 73$ Å). At the end of the data collection, the first 50 frames of data were recollected to establish that the crystal had not deteriorated during the data collection. The data frames were integrated using the SAINT program and merged to give a unique data set for structure determination. Absorption correction was performed by using SADABS.[17] The structure was solved by direct methods and refined by full-matrix least-squares methods on all F^2 data using the SHELXTL package (Bruker Analytical X-ray Systems). Non-hydrogen atoms were refined with anisotropic thermal parameters. Hydrogen atoms were included in calculated positions and refined with isotropic thermal parameters riding on those of the parent atoms.

Physical Measurements. Magnetic susceptibility data with an applied magnetic field of 1 T were collected using a Quantum Design MPMS-5S SQUID magnetometer. Temperature dependence was measured at every 1.0 K in the settle mode. The temperature scan rate was fixed to 0.1 K/min, and each measurement was performed 60 s after the temperature had stabilized. Magnetic data was corrected for the diamagnetism of a sample holder, and the diamagnetism of the sample was corrected using Pascal's constants. Photomagnetic experiments were carried out by using light from a DPSS laser (532 nm with 10 mW, Opto Tech 532.200.KE.01 and 808 nm with 10mW, Intelite I808-120G-CAP) or a Xe lamp (PE·ILC CERMAX Xenon illuminator LX300). The light was guided into the SQUID magnetometer via a flexible optical fiber (Newport F-MBD; 3 m length, 1.0 mm core size, 1.4 mm diameter). Irradiation was performed on the ground sample inside the SQUID sample chamber at 5 K. One end of the optical fiber was placed 40 mm above the sample, and the other end was attached to a coupler (body, Newport M-F-916T; lens, M-10X) for the lasers. The temperature dependence of the magnetic susceptibilities after light irradiation was measured with a scan rate of 0.3 K/min. Mössbauer experiments were carried out using a ^{57}Co/Rh source in a constant-acceleration transmission spectrometer. The spectra were recorded in the range 20−270 K in both cooling and heating modes. The spectrometer was calibrated using a standard α-Fe foil. The sample for calorimetry was sealed in a gold-plated copper calorimeter vessel with helium and a saturated vapor of $MeNO_2$ under atmospheric pressure. The mass of the sample was 2.0978 g after the buoyancy correction, though it included a small amount of $MeNO_2$ physically adsorbed on the surface of the sample. The amount of absorbed $MeNO_2$ was determined to be 1 wt % by TG-DTA. The details of the adiabatic calorimeter used and its operations have been described elsewhere.[18] The net amount of **1** for the heat capacity measurement was, thus, determined to be 1.706 mmol. The heat capacity measurement was carried out by the so-called intermittent heating adiabatic method. The temperature increment by a single energy input (Joule heating) was less than 1% of the temperature. After the energy input was turned off, thermal equilibrium inside the vessel was attained within a normal time (1−10 min, depending on the temperature) outside the temperature region around the phase transitions. The sample contributed to the heat capacity by 19% of the total heat capacity including that of the vessel at 50 K, 15% at 100 K, and 19% at 200 K.

Results and Discussion

Synthesis and Structural Description at 293 K. The reaction of $[Fe(dpp)_2](BF_4)_2$ and $(Bu_4N)[Ni(mnt)_2]$ in $MeNO_2$ gave a dark green solution, which was allowed to stand at 5 °C to give black platelike crystals of **1** (yield of 61%). The X-ray crystal structure analysis was performed at 293 K. A molecular structure and crystal packing diagrams are depicted in Figure 1, and the selected interatomic distances are summarized in Table 1. **1** crystallized in the triclinic space group $P\bar{1}$. The asymmetric unit contains one $[Fe(dpp)_2]^{2+}$ cation, two $[Ni(mnt)_2]^-$ anions ($[Ni1]^-$ and $[Ni2]^-$), and one nitromethane molecule. The pyrazole rings of $[Fe(dpp)_2]^{2+}$ form stacks with the $[Ni2]^-$ moieties in the crystal structure (see Figure S1 in the Supporting Information). The nitromethane molecules are positionally disordered over at least two positions with different orientations, and they weakly interact with the $[Fe(dpp)_2]^{2+}$ cations through CH···O hydrogen bonds, forming a 3D network (Figure S2). The iron(II) ion has a distorted-octahedral coordination structure with six nitrogen atoms from the two tridentate dpp ligands. Fe−N bond lengths are in the range of 2.085(4)−2.171(4) Å, where axially compressed Jahn−Teller distortion was observed along the N1−Fe−N6 bond. Distortion of the coordination geometry from the ideal octahedron was quantified by using Σ parameters ($\Sigma = |90 - \theta|$ (in deg), where the θ value is the bite angle of the two coordinated ligands).[19] Larger Σ values, which signify larger distortions from the ideal octahedral coordination sphere, correspond to a weaker ligand field strength on an iron(II) ion. The relatively large Σ value of 157.9° for the central iron(II) ion in **1** suggests that the iron(II) ion is in the HS state at 293 K. $[Ni1]^-$ and $[Ni2]^-$ have square-planar structures with torsion angles of S1−S2−S3−S4 = 175.36° and S5−S6−S7−S8 = 176.31°, respectively. Coordination bond lengths are Ni1−S = 2.138(2)−2.142(2) Å and Ni2−S = 2.139(2)−2.145(2) Å. In **1** at 293 K, the $[Ni1]^-$ and $[Ni2]^-$ moieties are separated with interplane distances of 3.596 and 3.637 Å, respectively (Figure 1b,c), and they are regarded as monomeric radicals with $S = {}^1/_2$. Note that the stacking modes of $[Ni1]^-$ and $[Ni2]^-$ moieties depended upon the temperature, and the temperature variations led to monomer−dimer conversions of the nickel moieties (vide infra).

Magnetic Properties. Magnetic susceptibility measurements of **1** were performed in the temperature range of 5−270 K in cooling and heating modes, and the results are shown in Figure 2. In the temperature range of 270−180 K, the $\chi_m T$ values remained nearly constant (4.04 emu mol^{-1} K), suggesting that the HS iron(II) ion ($S = 2$) and two $[Ni(mnt)_2]^-$ anions ($S = {}^1/_2$) are magnetically isolated, constituting the high-temperature (HT) phase. Supposing that the g value of $[Ni(mnt)_2]^-$ anions is equal to 2.0, the iron(II) ion ($S = 2$) in **1** has a g_{Fe} value of 2.09. Upon further cooling, an abrupt decrease in the $\chi_m T$ values to zero started at 180 K, indicating the occurrence of a first-order phase transition from the paramagnetic HT phase to the diamagnetic low-temperature (LT) phase. The phase transition from the HT to the LT phase is associated with simultaneous spin state conversions on the iron(II) center and both $[Ni(mnt)_2]^-$

(17) Sheldrick, G. M. SADABSs: An Empirical Absorption Correction Program; Bruker Analytical X-ray Systems, Madison, WI, 1996.
(18) Yamamura, Y.; Saito, K.; Saitoh, H.; Matsuyama, H.; Kikuchi, K.; Ikemoto, I. *J. Phys. Chem. Solids* **1995**, *56*, 107.
(19) Guionneau, P.; Marchivie, M.; Bravic, G.; Létard, J.-F.; Chasseau, D. *J. Mater. Chem.* **2002**, *12*, 2546.

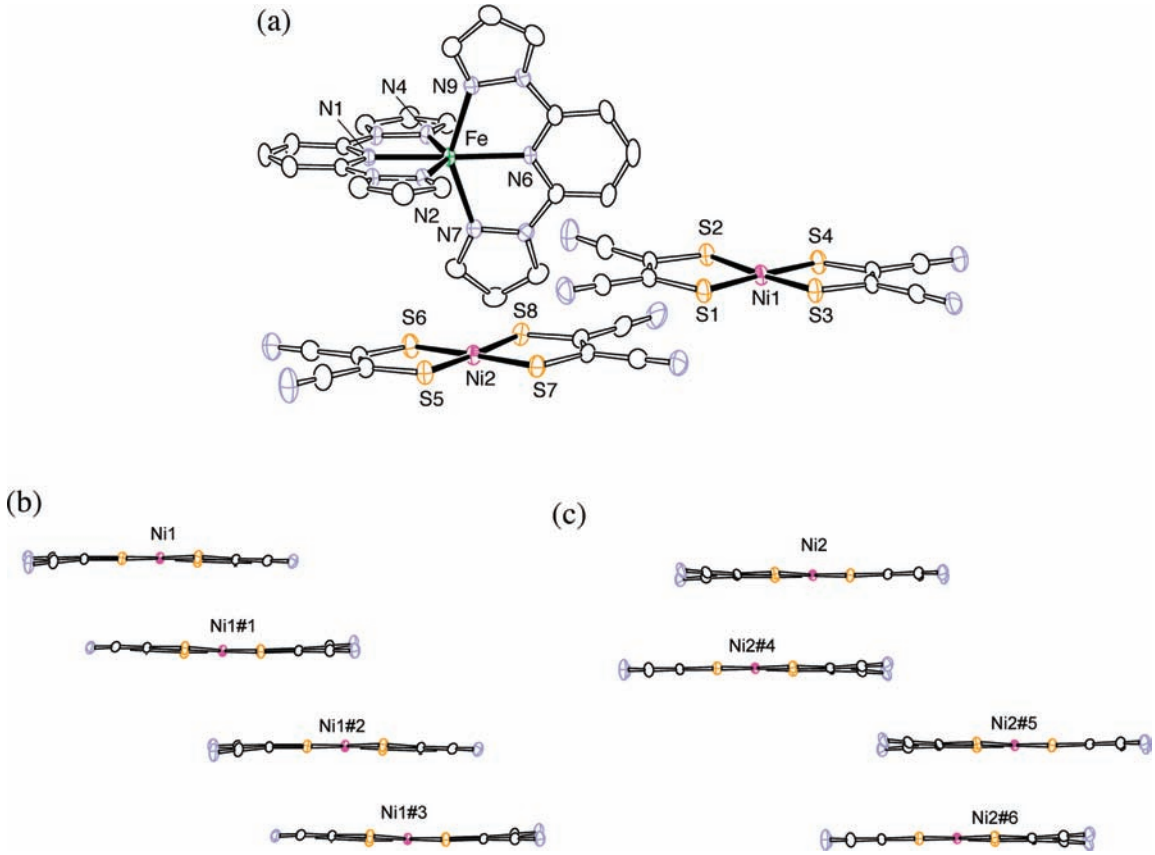

Figure 1. (a) ORTEP diagram of component molecules in **1** and stacking diagrams of (b) $[Ni1]^-$ and (c) $[Ni2]^-$ moieties along the *a* axis in **1** at 293 K. Key to symmetry operations: (#1) $2-x, 1-y, 1-z$; (#2) $1+x, y, z$; (#3) $3-x, 1-y, 1-z$; (#4) $2-x, 1-y, 2-z$; (#5) $1+x, y, z$; (#6) $3-x, 1-y, 2-z$.

Table 1. Selected Interatomic and Interplanar Distances (Å)

	293 K (↓)[a]	200 K (↓)[a]	140 K (↓)[a]	205 K (↑)[b]
Fe−N1	2.085(4)	2.127(3)	1.900(3)	2.101(6)
Fe−N2	2.186(4)	2.204(3)	1.977(3)	2.150(7)
Fe−N4	2.160(4)	2.185(3)	1.981(3)	2.155(6)
Fe−N6	2.098(4)	2.129(3)	1.902(3)	2.104(6)
Fe−N7	2.171(4)	2.197(3)	1.958(4)	2.132(7)
Fe−N9	2.153(4)	2.172(3)	1.968(4)	2.156(7)
Fe−N (av)	2.142(4)	2.169(3)	1.948(3)	2.133(7)
Σ (deg)	157.9	168.5	94.1	148.8
Ni1−S (av)	2.140(2)	2.144(1)	2.144(1)	2.141(1)
Ni2−S (av)	2.143(2)	2.147(1)	2.150(1)	2.140(2)
S3···S4 (within dimers)	4.225	4.085	3.737	3.962
S1···S2 (between dimers)	4.216	4.163	3.987	3.848
S7···S8	4.445	4.398	4.046	4.019
interplane dist				
within $[Ni1]^-$ dimers	3.596	3.503	3.436	3.554
between $[Ni1]^-$ dimers	3.671	3.629	3.538	3.647
within $[Ni2]^-$ dimers	3.637	3.583	3.445	3.333

[a] Measured after cooling from 300 K. [b] Measured after heating from 140 K.

($[Ni1]^-$ and $[Ni2]^-$) anions. That is, the iron(II) ion undergoes the SCO from the HS ($S = 2$) to the LS ($S = 0$) states, and the monomeric $[Ni1]^-$ and $[Ni2]^-$ moieties in the HT phase become dimerized to a diamagnetic state in the LT phase. This was in good agreement with the changes of interplanar distances for $[Ni1]^-$ and $[Ni2]^-$ dimers, which shorten from 3.596 and 3.637 Å at 293 K to 3.436 and 3.445 Å at 140 K (vide infra). The structural changes will be discussed in detail below. When the temperature was increased from 160 to 270 K in the heating mode, the $\chi_m T$ values increased in a four-step manner centered at 175.5, 186.5, 194.0, and 244.0 K, reaching at the HT phase

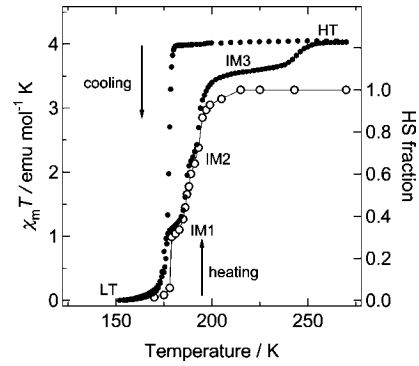

Figure 2. $\chi_m T$ versus T plot (filled circles) and temperature dependence of HS fractions (open circles), obtained by Mössbauer measurements, in the heating mode. The line is a guide for the eye.

via three intermediate IM1, IM2, and IM3 phases, which were confirmed by calorimetric experiments described below. The $\chi_m T$ value in the IM1 phase is 1.18 emu mol^{-1} K at 181 K, which corresponds to the value (1.09 emu mol^{-1} K) expected for one-third of the iron(II) ions ($S = 2$, $g_{Fe} = 2.09$) being in the HS state and both nickel moieties remaining diamagnetic and dimerized in the IM1 phase. This was confirmed by Mössbauer spectra and structure analysis at 180 K. The IM2 phase, which appears in a very narrow temperature range, has an $\chi_m T$ value of 2.18 emu mol^{-1} K at 189 K, suggesting that further spin transition occurred on the iron(II) sites. The subsequent phase transition occurred to the IM3 phase, for which the $\chi_m T$ value was 3.61 emu mol^{-1} K at 226 K. The $\chi_m T$ value in the IM3 phase corresponds to the value (3.66 emu mol^{-1}

K^{-1}) expected for one noncorrelated HS iron(II) ion and one nickel complex anion ($S = {}^1/_2$). The interplanar distance within the $[Ni2]^-$ dimers remains short (3.333 Å), in contrast with those (3.554 and 3.647 Å) for the $[Ni1]^-$ moieties at 205 K (vide infra), meaning the monomeric and dimeric forms of $[Ni1]^-$ and $[Ni2]^-$ moieties, respectively, in the IM3 phase. **1** showed a four-step phase transition from the LT phase to the IM1, IM2, IM3, and HT phases in the heating mode. The multistepped thermal hysteresis suggested multiple bistability of **1**, in which the HT phase can coexist with both the IM1 the and IM2 phases at 181 and 190 K and with the IM3 phase in the temperature range of 206−234 K. Note that the temperature profiles of the $\chi_m T$ values were reproduced in subsequent temperature scans and at different temperature scan rates (0.1−1.0 K/min) (Figure S3). The different temperature profiles of the $\chi_m T$ products in the cooling and heating modes are due to monotropism, which has been observed in polymorphic solids and liquid crystals[20] as well as in $[Cp_2Co][Ni(L)_2]$.[13] The $\chi_m T$ values were monitored at 215 and 185 K in the cooling process and at 180 and 215 K in the heating process, and no obvious changes of the $\chi_m T$ values were observed for 6 h, meaning that each state is stable within the experimental period. It should be noted that the multistepped phase transition behavior in **1** is quite sensitive to the loss of the crystallinity due to partial removal of crystal solvent molecules and the spin transition behavior is completely different from that in the crystalline sample (Figures S4 and S5).

Variable-Temperature ^{57}Fe Mössbauer Spectra. Variable-temperature ^{57}Fe Mössbauer spectra of **1** were measured to characterize the spin state of the iron(II) center in each phase. The temperature dependence of the HS fractions, which was calculated from the peak area ratios, is plotted in Figure 2, and selected spectra are shown in Figure 3. Mössbauer parameters are summarized in Table S2. The HS fractions, estimated from Mössbauer spectra, showed a three-step change centered at 178, 187, and 193 K upon heating from 170 to 225 K, which corresponds to the phase transitions from the LS to the IM3 phase via IM1 and IM2 phases, and the transition temperatures agree well with those observed in the magnetic susceptibility measurements. Each Mössbauer spectrum at 270 and 185 K (HT phase) is composed of a quadrupole doublet with the Mössbauer parameters of $\delta = 1.00$ and $\Delta E_Q = 1.43$ mm s^{-1} (relative to the metallic iron) and $\delta = 1.05$ and $\Delta E_Q = 1.70$ mm s^{-1}, respectively, meaning that the iron(II) ion in the HT phase is in a HS state ($S = 2$). In the LT phase at 20 K, only a new quadrupole doublet with $\delta = 0.40$ and $\Delta E_Q = 0.76$ mm s^{-1}, characteristic of LS iron(II) species, was observed, suggesting that a complete spin transition from the HS to the LS states occurred in the LT phase. As the temperature was raised to 181 K (IM1) in the heating mode, an additional doublet with $\delta = 1.04$ and $\Delta E_Q = 1.66$ mm s^{-1}, indicative of HS iron(II), was observed. The peak area ratio of HS to LS iron(II) species is 0.32/0.68 at 181 K. Note that the $\chi_m T$ value at 181 K in the heating mode is 1.18 emu mol^{-1} K, and the value corresponds to an HS:LS ratio of 0.36:0.64 with a g_{Fe} value of 2.09 and diamagnetic nickel moieties. Magnetic and Mössbauer data suggested that one-third of the iron(II) centers have undergone SCO in the transition from LS to IM1 phases, and this excludes the occurrence of monomerization on the $[Ni]^-$ sites in the IM1 phase. As the temperatures were raised to 189 K (IM2 phase), the HS iron(II) peak intensity increased, and the peak area ratios

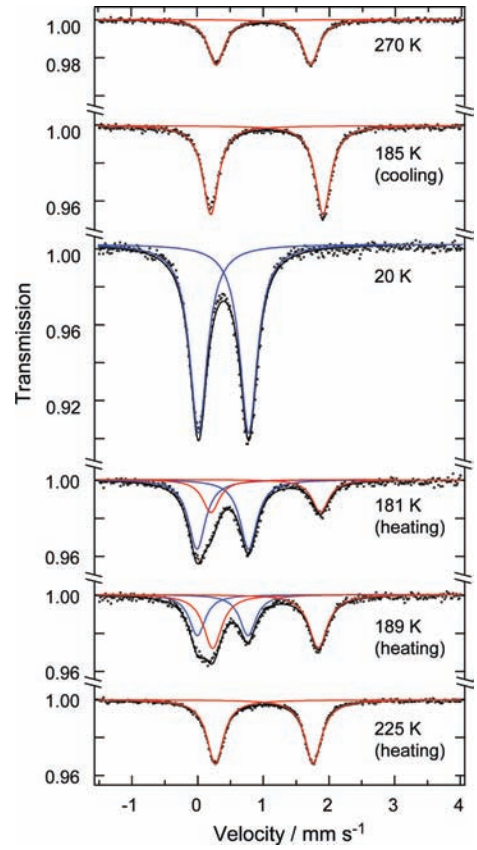

Figure 3. Selected ^{57}Fe Mössbauer spectra of **1**. The spectra were measured in the cooling and heating modes. The solid lines are Lorentzian curves calculated by using the parameters in Table S2. The isomer shift values are relative to metallic iron.

(HS/LS) became 0.60/0.40, where the $\chi_m T$ value (= 2.18 emu mol^{-1} K) at 189 K corresponds to an HS/LS ratio of 0.66/0.34. The results suggest that the IM2 phase contains two-thirds HS iron(II) ions and both $[Ni]^-$ sites in the dimeric and diamagnetic forms. At 225 K (IM3 phase), only the HS Fe(II) doublet was observed, indicating the completion of spin-state conversion on the iron(II) center in the IM3 phase. Note that the $\chi_m T$ value at 226 K was 3.61 emu mol^{-1} K, corresponding to the theoretical value (3.66 emu mol^{-1} K = 3.28 + 0.375 with $g_{Fe} = 2.09$ and $g_{Ni} = 2.00$) expected for the sum of the Curie constant of one HS iron(II) ion and one $S = {}^1/_2$ $[Ni]^-$ site. The results suggest that in the IM3 phase all iron(II) centers are in the HS state and half of the $[Ni]^-$ sites are monomerized.

Heat Capacity Measurements. The magnetic and Mössbauer data suggested multiple phase transitions with the three intermediate phases (IM1−IM3). Heat capacity (specific heat) measurements of **1** were carried out from 6 to 295 K (Figure 4), to confirm the thermodynamic stability of the phases. Note that the sampling for the heat capacity measurements was carried out under $MeNO_2$ vapor to perturb the release of the solvent molecules; therefore, the specific heat contains a small contribution from $MeNO_2$ which has been physically adsorbed on the surface of the sample. Four sharp anomalies of the latent heat were observed at 175, 187, 194, and 245 K, which strongly suggests the existence of four stable phases in addition to the room-temperature phase. Adiabatic calorimetry allows estimation of the enthalpy of transitions (transition enthalpy) by summing the energy inputs. Before the summation, a temporary interpolating curve (the dashed curve in Figure 4) was drawn for the facile estimation of excess energy. Figure 5 shows the

(20) Pardo, L. C.; Barrio, M.; Tamarit, J. L.; Salud, J.; López, D. O.; Negrier, P.; Mondieig, D. *Phys. Chem. Chem. Phys.* **2004**, *6*, 417.

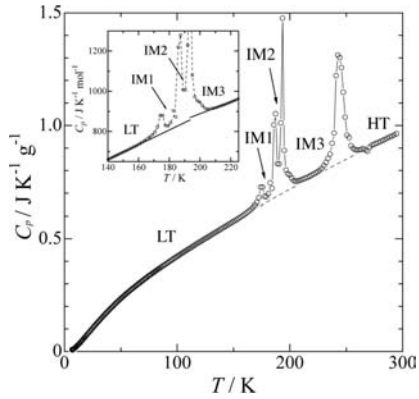

Figure 4. Observed heat capacity and molar heat capacity (inset) versus temperature plots of **1**. The dashed lines are temporary curves to estimate the sum of the energy input, and the solid (inset) lines were determined by extrapolating from the heat capacity of the LT and IM3 phases.

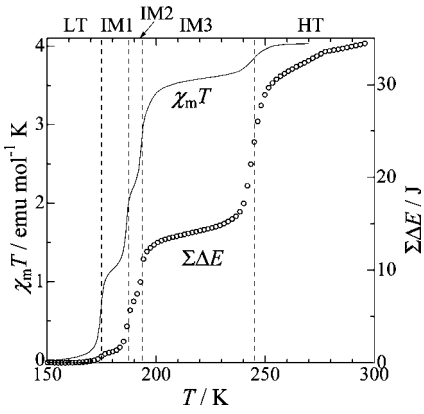

Figure 5. Cumulative sum of the energy inputs ($\sum\Delta E$) and the $\chi_m T$ versus temperature plots.

Table 2. Thermodynamic Parameters of **1**

transition	T_{trs}/K	$\Delta_{trs}H$/kJ mol^{-1}	$\Delta_{trs}S$/J K^{-1} mol^{-1}
LT → IM1	174.9	0.9	5
IM1 → IM2	187.4	3.2	17
IM2 → IM3	193.5	3.5	18
IM3 → HT	245.0	7.6	31

cumulative sum of energy inputs ($\sum\Delta E$) versus temperature, together with the $\chi_m T-T$ plot, where the integrated energy corresponding to the interpolating curve has been subtracted. The temperatures of the four sharp jumps in energy (175, 187, 194, and 245 K) are in agreement with those of the drastic jumps in $\chi_m T$.

The $\sum\Delta E$ versus T plot showed a gradual increase of the heat capacity changes in the temperature range of 252−275 K (Figure 5), which is due to "gradual" melting of the $MeNO_2$ absorbed on the surface of the sample. The increment of the heat capacity variations is consistent with the amount of adsorbed $MeNO_2$ estimated from the thermogravimetric measurements (Figure S6). Note that the contribution of the adsorbed $MeNO_2$ has no influence on the size of the energy jumps of the $\sum\Delta E$ value below the IM3 phase, because the melting/freezing temperature of $MeNO_2$ is 245 K. The enthalpy ($\Delta_{trs}H$) and entropy ($\Delta_{trs}S$) changes of the transitions were determined from the energy jumps of the $\sum\Delta E$ values at the phase transition temperatures, and the results are summarized in Table 2. The $\Delta_{IM3\rightarrow HT}H$ and $\Delta_{IM3\rightarrow HT}S$ values were corrected by subtracting the contribution of the absorbed $MeNO_2$, where the enthalpy of fusion of $MeNO_2$ is 9.7 kJ mol^{-1}.[21] The molar heat capacity of **1**, obtained by subtracting the heat capacity of the $MeNO_2$ in the solid state, is depicted in Figure 4 (inset).[21]

The combined entropy increment from the LT to the IM3 phases is $\Delta_{LT\rightarrow IM3}S = 40$ J K^{-1} mol^{-1}, which is 2 times larger than the value expected for the changes of spin multiplicity (R(ln 5 + ln 2) ≈ 20 J K^{-1} mol^{-1}, where the R is the gas constant). The base lines in the molar heat capacity versus temperature plot (Figure 4, inset), which were extrapolated from the LT and IM3 phases, did not cross at the transition temperatures. This suggests that the heat capacities are largely different before and after the transitions. The excess entropy contribution can be, therefore, attributed to the change of lattice vibrations upon the LT to the IM3 phase transitions, which has been often observed in first-order phase transitions of SCO systems.[22] The entropy change from the IM3 to HT phases, $\Delta_{IM3\rightarrow HT}S \approx 35$ J K^{-1} mol^{-1}, is also much larger than that of the spin manifold changes in the monomerization of the [Ni2] dimer (R ln 2 ≈ 5.8 J K^{-1} mol^{-1}). The excess entropy can be understood by the contribution of structural changes such as orientational disordering of the $MeNO_2$ molecules. The entropy change involved in the lowest anomaly (LT to IM1) is $\Delta_{LT\rightarrow IM1}S$ = ca. 5.0 J K^{-1} mol^{-1}, which is only slightly larger than the spin contribution ($^1/_3R$ ln 5 ≈ 4.5 J K^{-1} mol^{-1}), where the spin conversion ratio on the iron site was estimated from the Mössbauer spectroscopic and magnetic susceptibility data. The difference (0.5 J K^{-1} mol^{-1}) is substantially smaller than the ideal entropy of mixing ($-R[^1/_3$ ln $^1/_3 + {}^2/_3$ ln $^2/_3)] \approx 5.3$ J K^{-1} mol^{-1}) of the HS and LS iron(II) ions. This strongly suggests that the HS iron(II) atoms are arranged with some periodicity in the IM1 phase, resulting in a superlattice structure.

We summarize the heat capacity experiments as follows: (1) the plateaus in the magnetic susceptibility certainly correspond to thermodynamic phases; (2) the entropies of the transitions contain significant contributions from the lattice degrees of freedom (such as lattice vibration), beyond those due to changes in the spin multiplicity; (3) the $\Delta_{IM3\text{-}HT}S$ value is expected to contain the entropy increment due to orientational disorder of the $MeNO_2$ molecules; (4) the small $\Delta_{LT\rightarrow IM1}S$ value implies that an ordered arrangement of HS and LS Fe ions in the IM1 phase exists. If this is the case, it can be regarded as clear evidence of strong and direct coupling between spin and lattice degrees of freedom in a SCO complex.

Variable-Temperature X-ray Crystal Structure Analyses. The thermodynamic results suggested two possibilities concerning the structures of the low-temperature phases: the ordered arrangement of HS and LS iron(II) ions in the IM1 phase and the occurrence of the orientational order of the $MeNO_2$ molecules in the LT phase. To confirm the possibilities, further X-ray crystal structure analyses were carried out. First we checked the cell parameters of **1** in both cooling (250−140 K) and heating (140−210 K) modes (Figure S7), where measurement temperatures were calibrated using a thermocouple thermometer. In the cooling mode, the cell volume monotonically decreased as the temperature was lowered and showed a sudden decrease below 180 K, indicating a phase transition from the HT to the LT phase. In the heating mode, the cell volume was tripled at 179 K, suggesting the formation of long-range ordering in the IM1 phase.[9a,j,10] Upon a further increase of temperature up to 200 K, the cell parameters recovered to those

(21) Jones, W. M.; Giauque, W. F. *J. Am. Chem. Soc.* **1947**, *69*, 983.
(22) Sorai, M.; Seki, S. *J. Phys. Chem. Solids* **1974**, *35*, 555.

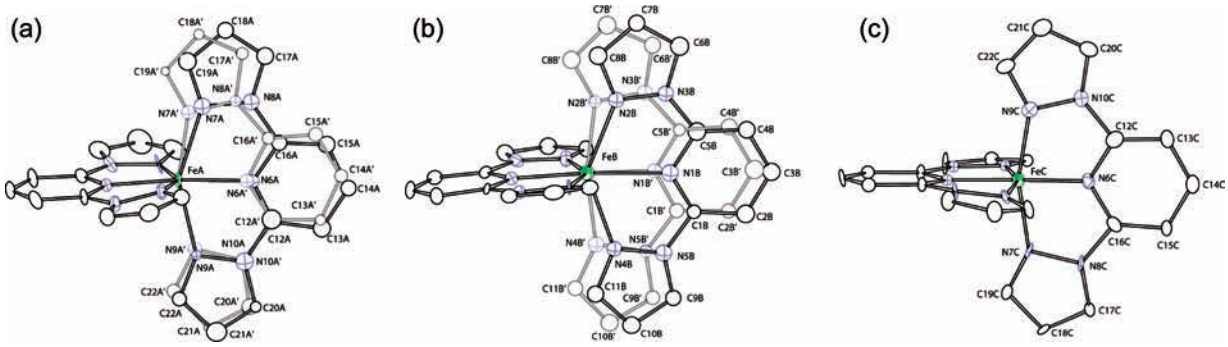

Figure 6. Structures of the complex cations: (a) [FeA]; (b) [FeB]; (c) [FeC]. The positionally disordered ligands are shown in gray.

of the original cell, due to the phase transition to the IM3 phase. We measured full sets of single-crystal diffraction data at 200 K (HT phase) and 140 K (LT phase) in the cooling mode and at 180 K (IM1 phase) and 205 K (IM3 phase) in the heating mode. X-ray structural data of the IM2 phase were not obtained, which is due to its narrow temperature range. Selected bond lengths are summarized in Table 1, and the stacking modes of $[Ni1]^-$ and $[Ni2]^-$ anions in the LT, IM1, IM3, and HT phases are depicted in Figure S5. The crystal structure at 200 K shows structural features similar to those at 293 K, except that the nitromethane molecule is not positionally disordered. The average coordination bond length about the iron(II) ion at 200 K is 2.169(3) Å, indicating that the iron(II) ion is in the HS state. The interplanar distances of the $[Ni1]^-$ and $[Ni2]^-$ moieties are 3.503 and 3.583 Å, respectively, and the stacking modes in the nickel complex anions remain unchanged at 293 and 200 K, suggesting that both radical moieties act as magnetically isolated monomers due to weak magnetic interactions within the dimers. In the LT phase at 140 K, the average coordination bond length around the iron(II) ion is shortened to 1.948(3) Å, characteristic of LS iron(II) ions. The stacking modes of $[Ni1]^-$ and $[Ni2]^-$ anions in the LT phase were apparently changed from the HT phase. The interplanar distances within dimers were shortened by 0.067 and 0.138 Å in $[Ni1]^-$ and $[Ni2]^-$ anions, respectively, suggesting that each $[Ni1]^-$ and $[Ni2]^-$ moiety is dimerized with a singlet ground state. The LT phase is diamagnetic, due to the dimerized $[Ni1]^-$ and $[Ni2]^-$ anions as well as the spin transition to the LS iron(II) state.

In the IM1 phase, superlattice reflections were clearly observed and were included in the structure analysis. The lattice parameters were drastically changed and the cell volume tripled, while the space group remained unchanged. The asymmetric unit contains three crystallographically independent iron(II) complexes ([FeA], [FeB], and [FeC]), six Ni moieties ([Ni1A], [Ni1B], [Ni1C], [Ni2A], [Ni2B], and [Ni2C]), and three nitromethane molecules (Figures 6 and S6), suggesting that the IM1 phase has long-range ordering with 3-fold periodicity. The average coordination bond length in [FeC] is 1.912(6) Å, suggesting that [FeC] is in the LS state. On the other hand, positional disorders on one of the two coordinating ligands were observed in the [FeA] and [FeB] cations (Figure 6), and the population ratios of the two disordered ligands were 0.64:0.36 and 0.58:0.42, respectively. The average coordination bond lengths in [FeA] and [FeB] are 2.08 and 2.09 Å, respectively, which deviate from the typical coordination bonds for LS and HS iron(II) species. Supposing that the average coordination bond length varies linearly with the population of HS and LS iron(II) species and their typical coordination bond lengths are 2.16 and 1.95 Å, respectively, the HS:LS ratios in the [FeA] and [FeB] sites were estimated to be 0.62:0.38 and 0.66:0.34. The overall HS:LS ratio including [FeA], [FeB], and [FeC] is ca. 0.40:0.60 in the IM1 phase, which is in relatively good agreement with the values estimated from Mössbauer (0.32:0.68) and magnetic (0.33:0.67) data. In the $[Ni]^-$ moieties, [Ni1C]−[Ni1C], [Ni1A]−[Ni1B], [Ni2A]−[Ni2B], and [Ni2C]−[Ni2C] pairs are dimerized with average interatomic distances of S3···S4 = 3.780 and 3.765 Å and S7···S8 = 3.948 and 4.042 Å for $[Ni1]^-$ and $[Ni2]^-$ moieties, respectively (Figure S8), and the values are close to those (S3···S4 = 3.737 Å, S7···S8 = 4.046 Å) in the LT phase. In spite of the low quality of the X-ray data in the IM1 phase, it was suggested that one-third of the iron(II) ions are in the HS state and Ni complex anions remain dimerized. The X-ray structure analysis of the IM1 phase suggested positional disorders of the HS and LS species on the [FeA] and [FeB] sites, in spite of the fact that an ordered arrangement of the iron sites in the IM1 phase was deduced from the small $\Delta_{LT\rightarrow IM1}S$ value. This might be due to the fact that the superlattice reflections corresponding to the 6-fold periodicity were missed in the diffraction data due to the low crystalinity in the IM1 phase.

In the IM3 phase at 205 K, the HS iron(II) ion has longer coordination bond lengths with Fe−N = 2.104(6)−2.156(7) Å and the interplanar distance of 3.554 Å in $[Ni1]^-$ dimers is closer to that in the HT phase, meaning that the iron(II) ion is in the HS state and $[Ni1]^-$ is monomeric in the IM3 phase. The $[Ni2]^-$ ions in the IM3 phase are separated by an interplanar distance of 3.333 Å, corresponding to the dimeric form. Accordingly, in the IM3 phase, the iron(II) ion is in a HS state ($S = 2$) and

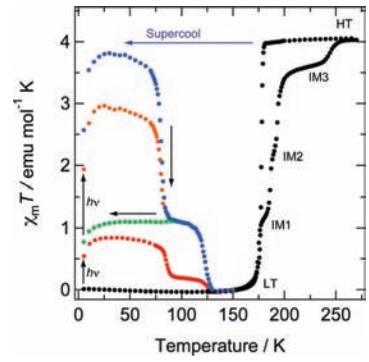

Figure 7. $\chi_m T$ variations upon thermal treatments and light irradiation experiments for **1**: temperature variation of 5−275 K before (black dots) and after light irradiation (at 532 nm) in the LT phase (red dots) at 5 K; rapid thermal quenching from 300 to 5 K followed by a temperature increase to 150 K (blue dots); metastable IM1 phase generated by heating the thermally quenched HT phase to 95 K and cooling back to 5 K (green dots) and after light irradiation at 5 K (orange dots).

Scheme 2. Phase Transition Diagram in **1**

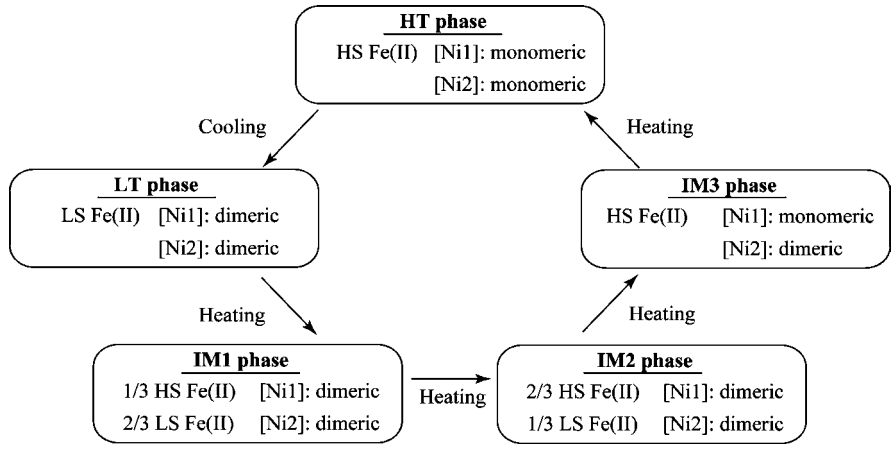

the $[Ni1]^-$ and $[Ni2]^-$ moieties have monomeric ($S = {}^1/_2$) and dimeric ($S = 0$) forms, respectively. The coordination structures of $[Ni(mnt)_2]^-$ (Ni1−S = 2.142(1)−2.146(1) Å, Ni2−S = 2.140(1)−2.159(1) Å at 140 K) are very similar in the full temperature range measured.

Supercooling State and Light-Induced Metastable States at Low Temperature. Supercooling and LIESST experiments were performed in the SQUID magnetometer to investigate possible conversion to the metastable HS state at low temperatures (Figure 7). When **1** was rapidly cooled down to 5 K from 300 K, the HT phase was trapped with the $\chi_m T$ value of 2.57 emu mol^{-1} K. As the temperature was raised, the $\chi_m T$ value increased to 3.82 emu mol^{-1} K at 30 K. Considering the orbital contribution of the HS iron(II) ion and the $\chi_m T$ value of 4.04 emu mol^{-1} K at 275 K, the HT phase was completely trapped by the supercooling to 5 K. Upon further heating, the supercooled HT phase relaxed to the LT phase in a two-step manner centered at 80 and 122 K (Figure 7, blue dots). The $\chi_m T$ value at 95 K (the first plateau) was 1.11 emu mol^{-1} K, which is close to the value (1.18 emu mol^{-1} K) of the IM1 phase. This suggests that the trapped HT states relaxed to the LT phase via the IM1 phase.

Light irradiation experiments were carried out in the LT and IM1 phases by laser light irradiation at a wavelength of 532 nm. When the sample in the LT phase was irradiated for 25 h at 5 K, the $\chi_m T$ value increased to reach a saturated value of 0.53 emu mol^{-1} K (Figure 7, red dots). In the subsequent temperature increase after turning off the light source, the $\chi_m T$ value increased and reached a maximum value (0.84 emu mol^{-1} K) at 32 K, and this suggests that 21% of the LT phase was converted to the metastable phase by light irradiation. Upon a further increase in temperature, the light-induced HT phase thermally relaxed to the LT phase in a two-step fashion at 85 and 123 K. The relaxation profile of the light-induced HT phase is similar to that of the supercooled HT phases, suggesting that the light irradiation induced both spin conversion on the iron(II) site and monomerization of the [Ni] moieties, giving a metastable HT phase. Note that the IM1 phase was not trapped by the light irradiation of the LT phase. The light irradiation experiment was also performed on the IM1 phase at 5 K, where the IM1 phase was generated by heating the thermally quenched HT phase to 95 K and cooling back to 5 K. The $\chi_m T$ values increased from 0.77 to 2.57 emu mol^{-1} K upon irradiation, and the $\chi_m T$ values decreased in the same manner in the supercooled HT phase (Figure 7. orange dots). The light conversion of the IM1 phase to the metastable HT phase was 70%, which was larger than that of the LT phase (21%). The lower light-conversion efficiency in the LT phase might be due to the shallower penetration depth of the green light compared with the IM1 phase.[2c] Note that the reverse conversion from the metastable HT or IM1 phases to the LT phase was not achieved by irradiation with 532 or 808 nm light or with white light.

Conclusion

The phase transitions in **1** are summarized in Scheme 2. In the cooling mode simultaneous spin-state conversions occurred both on the iron(II) ion and on the two $[Ni]^-$ anions, while in the heating process, successive phase transitions from the LT to the IM1, IM2, IM3, and HT phases were observed. The LT, HT, IM1, and IM3 phases were fully characterized by X-ray structure analyses and magnetic and Mössbauer data. In the IM1 phase, long-range ordering with 3-fold periodicity was observed and one-third of the iron(II) sites were in the HS state with the $[Ni]^-$ moieties dimerized. An additional one-third of the iron(II) sites undergo spin transitions from the LS to HS state during the phase transition from IM1 to IM2 phases. The remaining one-third of iron(II) ions as well as one of the Ni complex anions ($[Ni1]^-$) showed simultaneous spin-state conversion to generate the IM3 phase, which undergoes a phase transition to the initial HT phase associated with monomerization of the $[Ni2]^-$ moieties at higher temperature. In addition, the metastable HT phase can be trapped by rapid thermal quenching at 5 K and also by light irradiation of the LT phase and the metastable IM1 phase. **1** was regarded as a tristable (LT, IM1, and supercooled HT phases) and multiply bistable system.

Acknowledgment. This work was supported by a Grant-in-Aid for Scientific Research and for Priority Area "Coordination Programming" (area 2107) from the MEXT of Japan.

Supporting Information Available: CIF files, tables, and figures giving X-ray crystallographic data and additional structural and magnetic data. This material is available free of charge via the Internet at http://pubs.acs.org.

JA910122R